High-Resolution E-Beam Repair for Nanoimprint Templates

Marcus Pritschow[*a], Harald Dobberstein[b], Klaus Edinger[b], Mathias Irmscher[a], Douglas J. Resnick[c], Kosta Selinidis[c], Ecron Thompson[c], Markus Waiblinger[b]
[a]IMS Chips, Allmandring 30a, D-70569 Stuttgart, Germany;
[b]Carl Zeiss SMS GmbH, Carl Zeiss Promenade 10, D-07740 Jena, Germany;
[c]Molecular Imprints, Inc., 1807-C West Braker Lane, Austin, TX 78758, USA

ABSTRACT

UV nanoimprint lithography (UV-NIL) is a high-throughput and cost-effective patterning technique for complex nano-scale features and is considered a candidate for CMOS manufacturing at the 22nm node and beyond. To achieve this target a complete template fabrication infrastructure including inspection and repair is needed. Due to the 1X magnification factor of imprint lithography the requirements for these steps are more challenging compared to those for 4X photomasks. E-beam repair is a very promising repair technology for high-resolution imprint templates. It combines the advantages of precise beam placement using fine resolution images and damage free repair by electron beam induced chemical reactions. In this work we performed template repair using a new test stand with improved beam and stage stability. Repeatability of 3D pattern reconstruction with main focus on shrunk lateral repair dimensions and height control was investigated. The evaluation was done on various features in a 40nm half pitch design. Additionally, the resolution capability of the new hardware was examined on selected programmed defects in a 32nm half pitch design. A first qualitative examination of the repaired template was done using top-view SEM images taken from the test stand before and after repair. The repaired template was then imprinted on 300mm silicon wafers, and the imprinted repaired defects were analyzed using a SEM Zeiss Ultra 60.

Keywords: Nanoimprint Lithography, Template, Repair

1. INTRODUCTION

UV nanoimprint lithography (UV-NIL) is a high-throughput and cost-effective patterning technique for complex nano-scale features and is considered a candidate for CMOS manufacturing at the 22nm node and beyond. The manufacturing of templates with full-field flash gate layers using state-of-the-art variable shaped beam (VSB) pattern generators and commercially available resists have already been demonstrated. The results approached the specifications for the 32nm node requests in terms of resolution, line edge roughness, placement and uniformity [1]. Recent improvements in template patterning using VSB tools showed the capability towards full-field templates for CMOS device manufacturing below the 32nm half pitch [2]. However, a successful integration into CMOS fabrication lines requires a complete template fabrication infrastructure including inspection and repair. Due to the 1X magnification factor of imprint lithography the requirements for these steps are more challenging compared to those for 4X photomasks.

E-beam repair is a very promising repair technology for high-resolution imprint templates. It combines the advantages of precise beam placement using fine resolution images and damage free repair by electron beam induced chemical reactions. Recently, we demonstrated template repair using a dedicated e-beam repair test stand [3]. Programmed defects with various shapes and sizes were successfully repaired by application of recipes specifically tailored for NIL repair requirements. This paper continues our previous work involving a new test stand with improved beam and stage stability. Repeatability of 3D pattern reconstruction with main focus on shrunk lateral repair dimensions and height control was investigated. Additionally, the resolution capability of the improved hardware was examined on selected programmed defects in order to address possible requirements for imprint repair tools of future technology nodes. The repaired template was imprinted on 300mm silicon wafers, and the printed repaired defects were analyzed using SEM inspection.

[*] pritschow@ims-chips.de, phone: +49-711-21855-420, fax: +49-711-21855-111

2. EXPERIMENTAL

A template with programmed defects has been manufactured by Dai Nippon Printing. The patterns were exposed by using a JEOL 9300 Gaussian beam pattern generator. ZEP520A resist was chosen as the positive imaging resist. After development, the chromium and fused silica were etched using Cl_2/O_2 and fluorine-based chemistry, respectively. Mesa lithography and a mesa etch process, followed by a dice and polish step were employed to create a finished 65mm × 65mm template.

The test pattern consisted of an array of three different half pitches: 48nm, 40nm and 32nm. For each size, three pattern types were designed: SRAM Metal 1, contact hole array, and a dense line/space pattern. For each feature type, multiple programmed defects were introduced into the pattern. The details are shown in Figure 1. As an example for the 40nm lines and spaces, twelve incremental programmed defect sizes were inserted, starting at 5nm and ending at 60nm. Mousebites included three repeats in the horizontal and vertical directions. Extension defects were inserted in the same fashion. Examples of mousebite defects for the three pattern types are shown in Figure 2, SEM images of these defects on the template are shown in Figure 3. These programmed defects were extensively characterized using electron beam inspection tools prior to the repair experiments [4]. In this work we made repairs to a set of identical mousebite and missing contact hole defects in the 40nm half pitch design to investigate precision and repeatability of the e-beam repair process.

E-beam repair combines the energy of an incident electron beam with an appropriate precursor gas. Depending on the precursor chemistry, a reaction is induced by the focused electron beam. This leads to a deposition caused by fragmentation of precursor molecules or an etch reaction between the absorbed molecules and the substrate material, resulting in volatile products. Since the reaction is confined only to the area exposed by the electron beam, this technique allows high-resolution nanostructuring. The repair structure is derived by comparing a high-resolution image of the defective area with the same image of a non-defective area. The repair shape is generated as the difference of these two images, and adjusted for processing purposes.

The repair experiments were performed on a new e-beam repair test stand with improved beam and stage stability. It is equipped with a high-resolution electron beam column with very small beam spot size which is required for this application. The implemented charge compensation and drift correction enable advanced specifications for placement accuracy and reproducibility. In order to achieve better beam control during the repair process the overall system noise could be further reduced by extra vibration and acoustic damping in combination with improved temperature stability. An improved state-of-the-art laser interferometer controlled stage provides better positioning performance and stability.

Imprinting of the template with the programmed and partially repaired defects was performed by using a Molecular Imprints Imprio 300 imprint tool. A Drop-On-Demand method was employed to dispense the photo-polymerizable acrylate based imprint solution in field locations across a 300mm silicon wafer. The imprint mask was then lowered into liquid-contact with the substrate, displacing the solution and filling the imprint field. UV irradiation through the backside of the mask cured the acrylate monomer. The process was then repeated to completely populate the substrate. Details of the imprint process have previously been reported [5].

A first qualitative examination of the repaired template was done using top-view SEM images taken from the repair rest stand before and after repair. A more detailed analysis of repaired features was done on imprinted features using a Zeiss Ultra 60.

3. RESULTS AND DISCUSSION

3.1 Repair results on the template

Since the template only consists of quartz no endpoint detection system can be used during e-beam etch repair. For this reason we pre-characterized the etch rate to determine the repair time and adjusted tool parameters of the test stand. The parameters were kept constant throughout the experiments to evaluate the repeatability of the etch repair process. We made repairs to identical mousebite defects in the 40nm half pitch design for dense line and SRAM Metal 1 patterns. The chosen defect sizes were $40\times60nm^2$, $40\times50nm^2$ and $40\times40nm^2$. Due to the design and implementation of defects in the 40nm half pitch contact hole arrays the overlapping parts of larger defects only affected the size of an adjacent hole in the array. There was always one complete missing hole with 40nm diameter in the center of the array for the chosen

defect sizes. The SEM images in Figure 5 illustrate the increasing hole size above a centered defect for decreasing defect size.

Figure 4 shows a line/space and Metal 1 pattern with a $40\times50nm^2$ mousebite defect in one of the trenches and repaired patterns on three different locations. In both cases the placement of the repaired sections into the pattern was very accurate with good line width control. Figure 5 shows SEM images of a hole array with a $40\times40nm^2$ missing contact defect in its center and a set of six different arrays after repair. Some of the repaired holes are not exactly positioned in the center of the array because the repair areas were manually placed into the pattern before applying the pattern copy method. In this example all missing center holes were successfully etched into the template without any significant lateral dimensional deviation.

3.2 Analysis of repaired defects on wafer imprints

Following the imprinting on 300mm silicon wafers, SEM images were taken in the programmed defect areas. At first, repaired line features were investigated. Figure 6 shows SEM images of a 40nm half pitch line/space and Metal 1 pattern after repair of a $40\times50nm^2$ mousebite defect and three different imprinted patterns. In the Metal 1 patterns the location of the defect is mirrored in x relative to the template images, because of the imprint process. The example top-view SEM images of the imprints show good 2D replication fidelity for all repaired defects. In order to get the height information of the imprinted features we made tilted high-magnification SEM images of imprinted line/space and Metal 1 patterns after template repair (Figure 7). In the shown examples the repaired locations are slightly higher than the rest of the printed lines. It indicates that the etch time during template repair was longer than necessary. Nevertheless, the results show equal height of all repaired line defects within a set of identical defects and no influence of pattern type could be observed. The height deviation can easily be corrected by adjusting the etch time.

Analysis of repaired 40nm half pitch contact hole arrays were done by examining 18 imprints resulting in pillar arrays. Three hole arrays after repairs of a $40\times40nm^2$ missing contact hole in each pattern and imprints of these patterns on 18 different locations with identical defect size are shown in Figure 8. All repaired defects were clearly imprinted and were not damaged during the imprint process. The example top-view SEM images of the imprints show again good 2D replication fidelity. As previously discussed the smaller holes for certain defect sizes were neglected in this study. Similar to the line defects tilted high-magnification SEM images of imprinted pillar arrays after template repair were analyzed to get an impression of the pillar height (Figure 9). The SEM images show equal shape and size of all repaired pillars. The reason for the different lateral dimensions at the bottom and at the top of all repaired pillars is unknown yet and is subject of further investigations.

CD measurements to generate repeatability data were done on 18 imprinted pillar arrays using a SEM Zeiss Ultra 60. Width of repaired center pillars was measured in x and y directions by manual placing the measurement cursors. The mean values of all 18 repaired pillars yielded $x = 44.43nm$ ($3\sigma = 3.96nm$) and $y = 45.21nm$ ($3\sigma = 2.95nm$). Random pillars in the array were measured as references and were in the range of 39 to 41nm.

A more detailed 3D analysis of repaired defects would be possible by performing cross-section SEM analysis on specially designed cleavable patterns or by using high-resolution AFM analysis. Both were not available for this study and could be done in future repair studies.

Finally, the resolution capability of the new hardware was investigated by applying repair processes used for 40nm half pitch features to selected mousebite defects in the 32nm half pitch SRAM Metal 1 design. Repair examples of a $32\times32nm^2$ mousebite defect on two different locations are shown in Figure 10. Similar to the 40nm half pitch design the placement of the repaired sections was very accurate with good line width control.

4. CONCLUSION

In this work we successfully demonstrated e-beam repair processes on 1X templates by using a new test stand with improved beam and stage stability. A detailed repair evaluation on various 40nm features was performed and very good line width and positioning accuracy of the repaired features could be achieved. All repaired defects could be imprinted on 300mm silicon wafers without any pattern degradation. The imprint results showed very reproducible feature height

on all repaired features. The slight off-target values that were seen after repair can be corrected by a better adjusted etch process. Resolution capability of the new hardware was demonstrated applying e-beam repair to a 32nm half pitch design. The reason for observed footing on 40nm pillars resulting from imprints of repaired contact hole arrays is not yet understood and investigations to explain this effect are on-going. In addition, repairs to defects with smaller lateral dimensions are necessary in order to achieve repair requirements for future technology nodes. In summary, the results of our study show that e-beam repair is a very promising repair technology for high-resolution imprint templates.

ACKNOWLEDGEMENTS

The authors would like to thank Petra Spies from Carl Zeiss SMS GmbH for performing e-beam template repair. This work has been supported by the MEDEA+ 2T305 FANTASTIC project, the German Federal Ministry for Education and Research and by the Ministry of Economic Affairs of Baden-Wuerttemberg.

REFERENCES

1. Yeo, J., Kim, H., and Eynon, B., "Full-field imprinting of sub-40 nm patterns," Proc. SPIE 6921, 692107 (2008).
2. Sasaki, S., Hiraka, T., Mizuochi, J., Fujii, A., Sakai, Y., Sutou, T., Yusa, S., Kuriyama, K., Sakaki, M., Morikawa, Y., Mohri, H., and Hayashi, N., "UV-NIL template making and imprint evaluation," Proc. SPIE 7271, 72711M (2009).
3. Pritschow, M., Boegli, V., Butschke, J., Irmscher, M., Resnick, D., Sailer, H., Selinidis, K., and Thompson, E., "Evaluation of e-beam repair for nanoimprint templates," Proc. SPIE 7122, 71222L (2008).
4. Selinidis, K., Thompson, E., McMackin, I., Sreenivasan, S.V., and Resnick, D.J., "High-resolution defect inspection of step and flash imprint lithography for 32nm half pitch patterning," Proc. SPIE 7271, 72711W (2009).
5. Choi, B.J., Meissl, M.J., Colburn, M., Bailey, T.C., Ruchhoeft, P., Sreenivasan, S. V., Prins, F., Banerjee, S.K., Ekerdt, J.G., and Willson, C.G., "Layer-to-layer alignment for step and flash imprint lithography," Proc. SPIE 4343, 436 (2001).

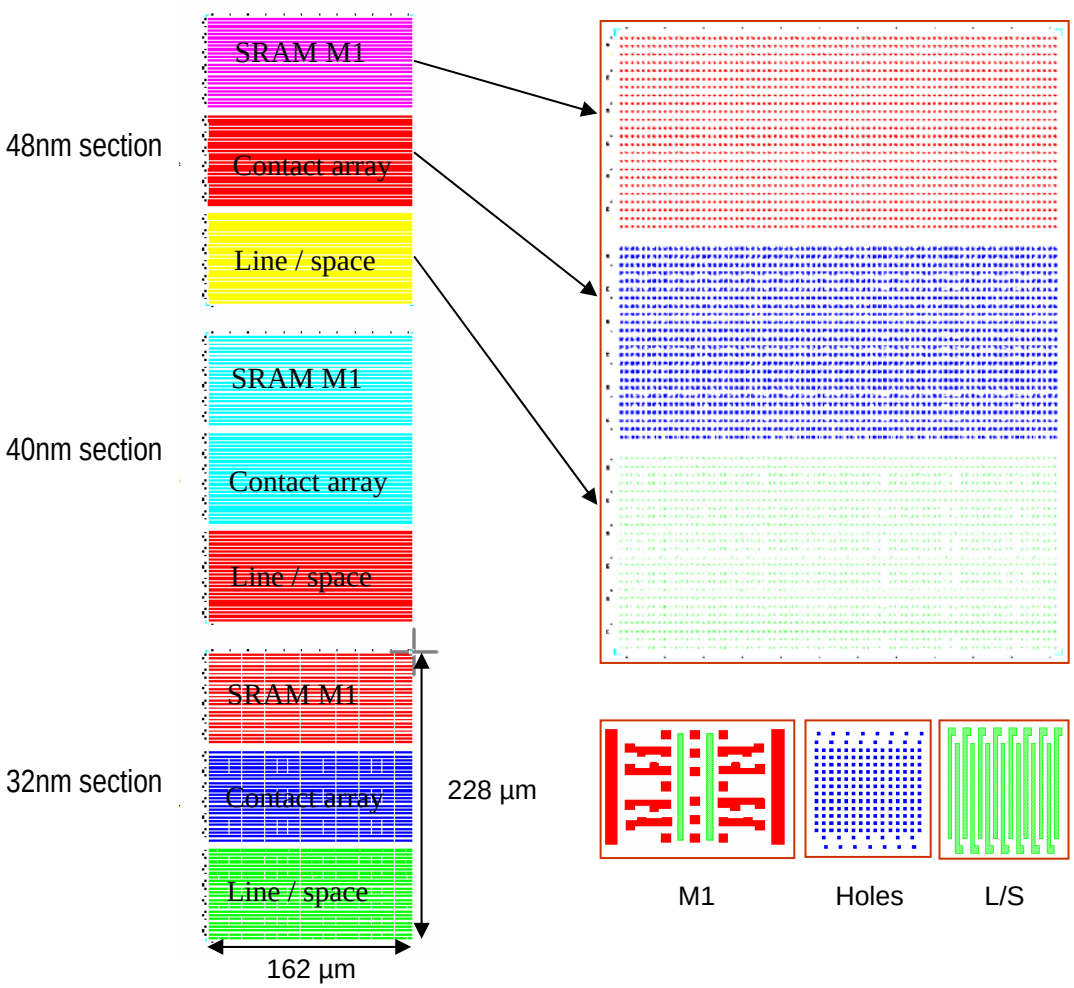

Figure 1. Programmed defect layout.

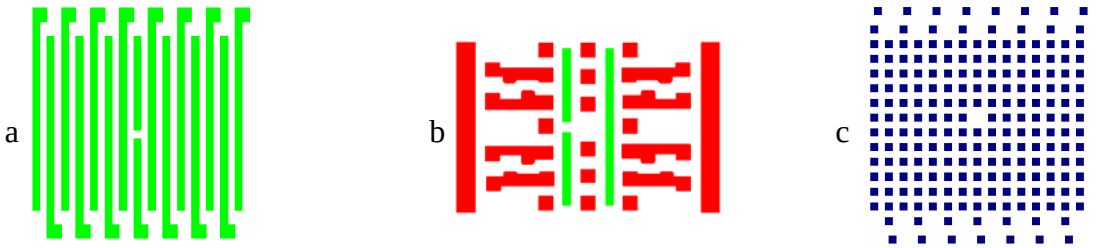

Figure 2. Two types of programmed defects in the layout: a) mousebite defect in the line/space pattern, b) mousebite defect in the SRAM Metal 1 cell, c) missing contact hole defect in the hole array.

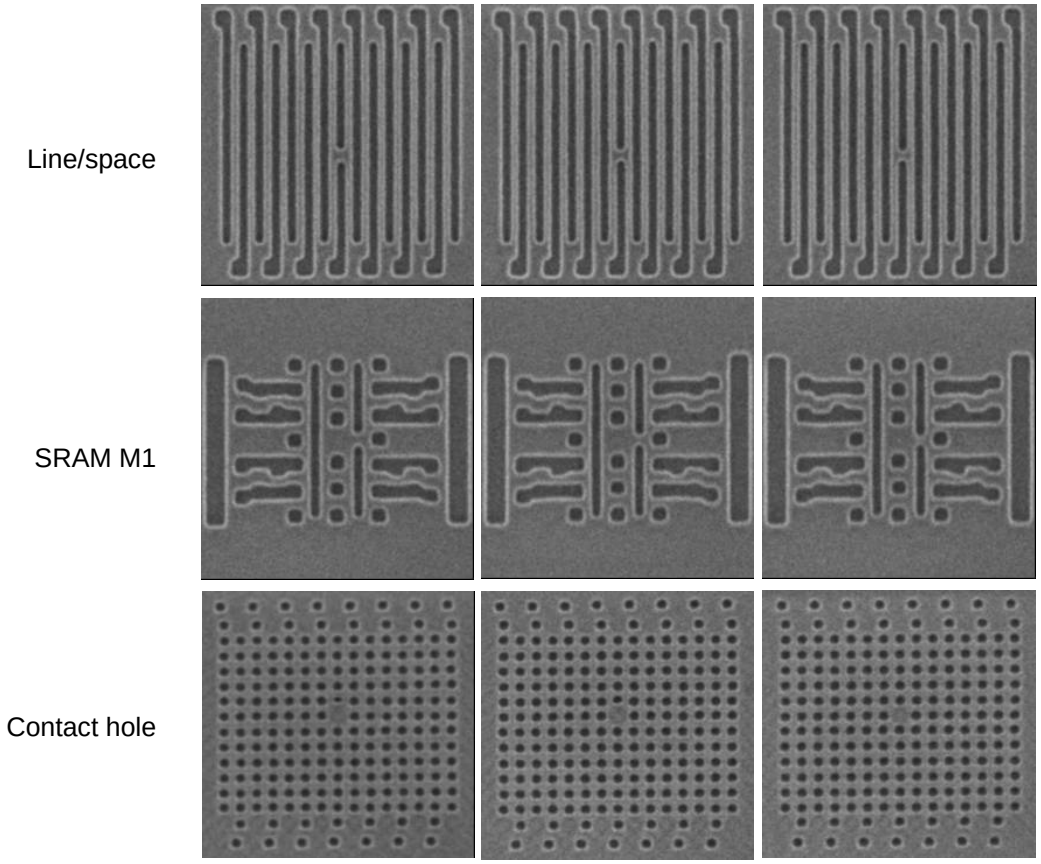

Figure 3. SEM images of programmed defects in the 40nm half pitch design on the template: a) line/space pattern, b) SRAM Metal 1 cell and c) contact hole array. In the contact hole design the smaller holes above the center defect appear due to the implementation of programmed defects larger than 40×40nm^2.

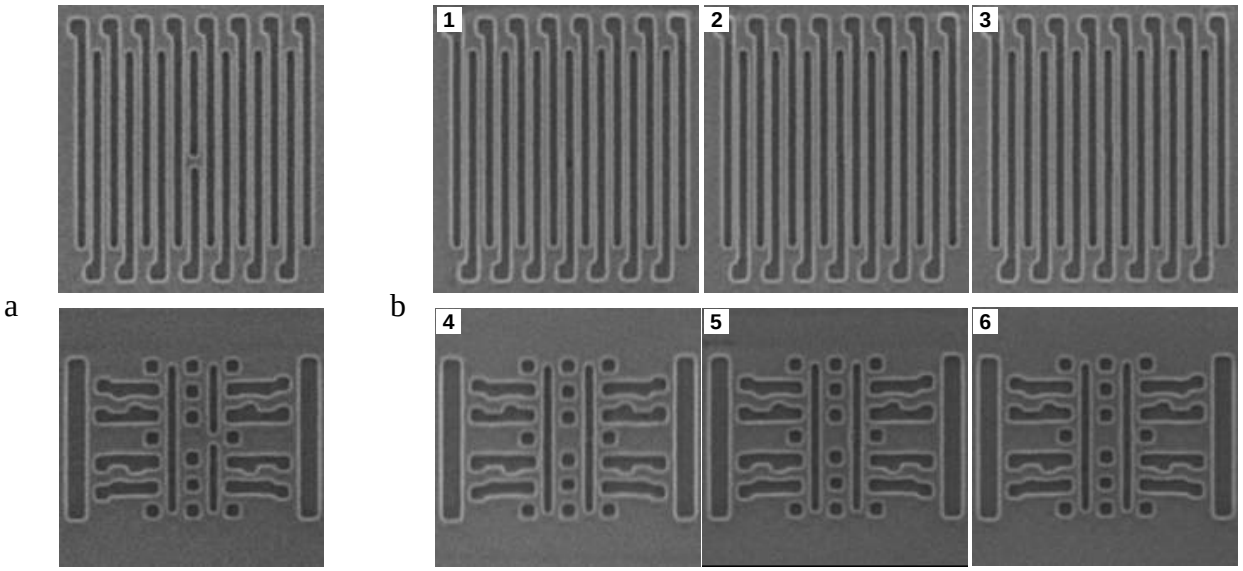

Figure 4. a) SEM images of a mousebite defect in the 40nm line/space and SRAM Metal 1 pattern before repair. b) SEM images of identical 40×50nm^2 mousebite defects after repair at three different locations.

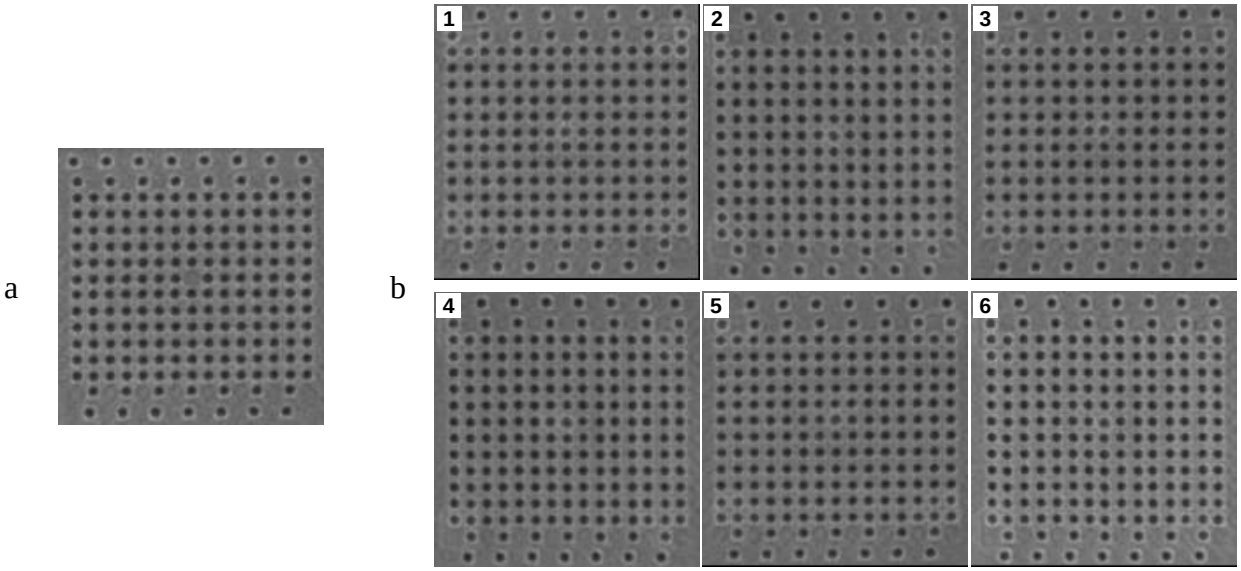

Figure 5. a) SEM image of a missing contact hole defect in the 40nm design before repair. b) SEM images of six identical 40×40nm^2 contact hole defects after repair.

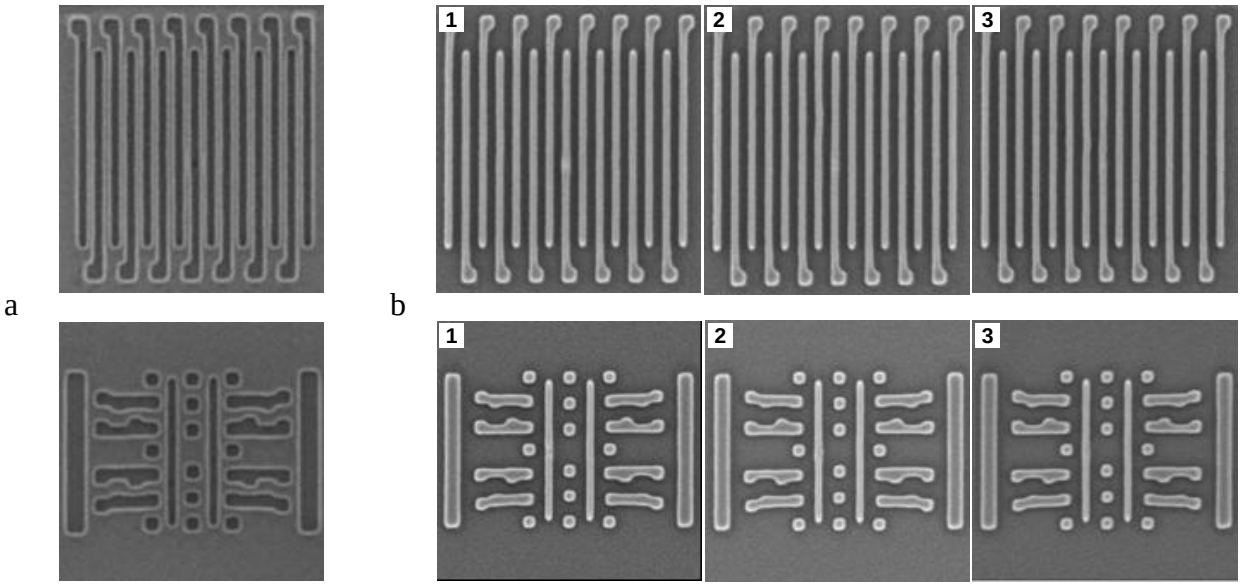

Figure 6. a) SEM images of a repaired 40×50nm^2 mousebite defect in the 40nm line/space and SRAM Metal 1 pattern. b) Imprints of three different repaired defect patterns with identical defect size.

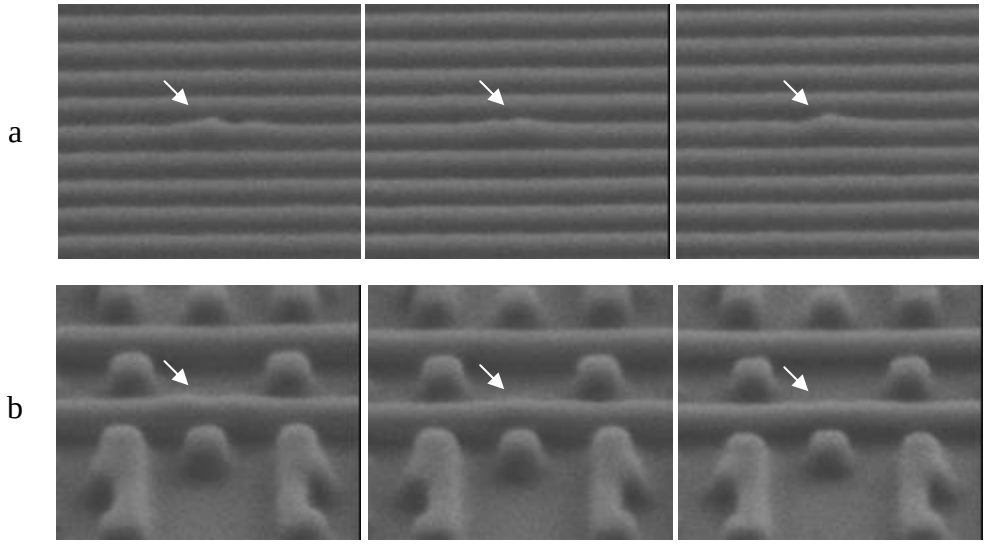

Figure 7. Tilted high-magnification images of imprints of repaired identical defects in the 40nm half pitch designs for three line/space patterns (a) and SRAM Metal 1 patterns (b).

a

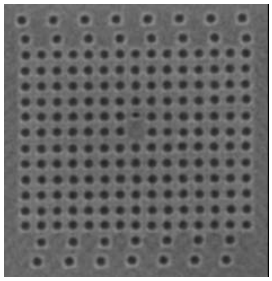

Defect site #1

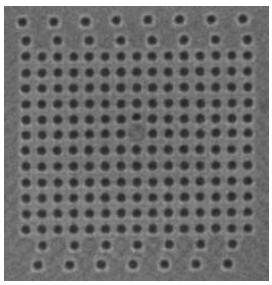

Defect site #7

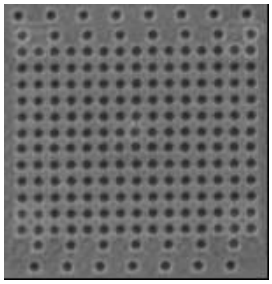

Defect site #13

b

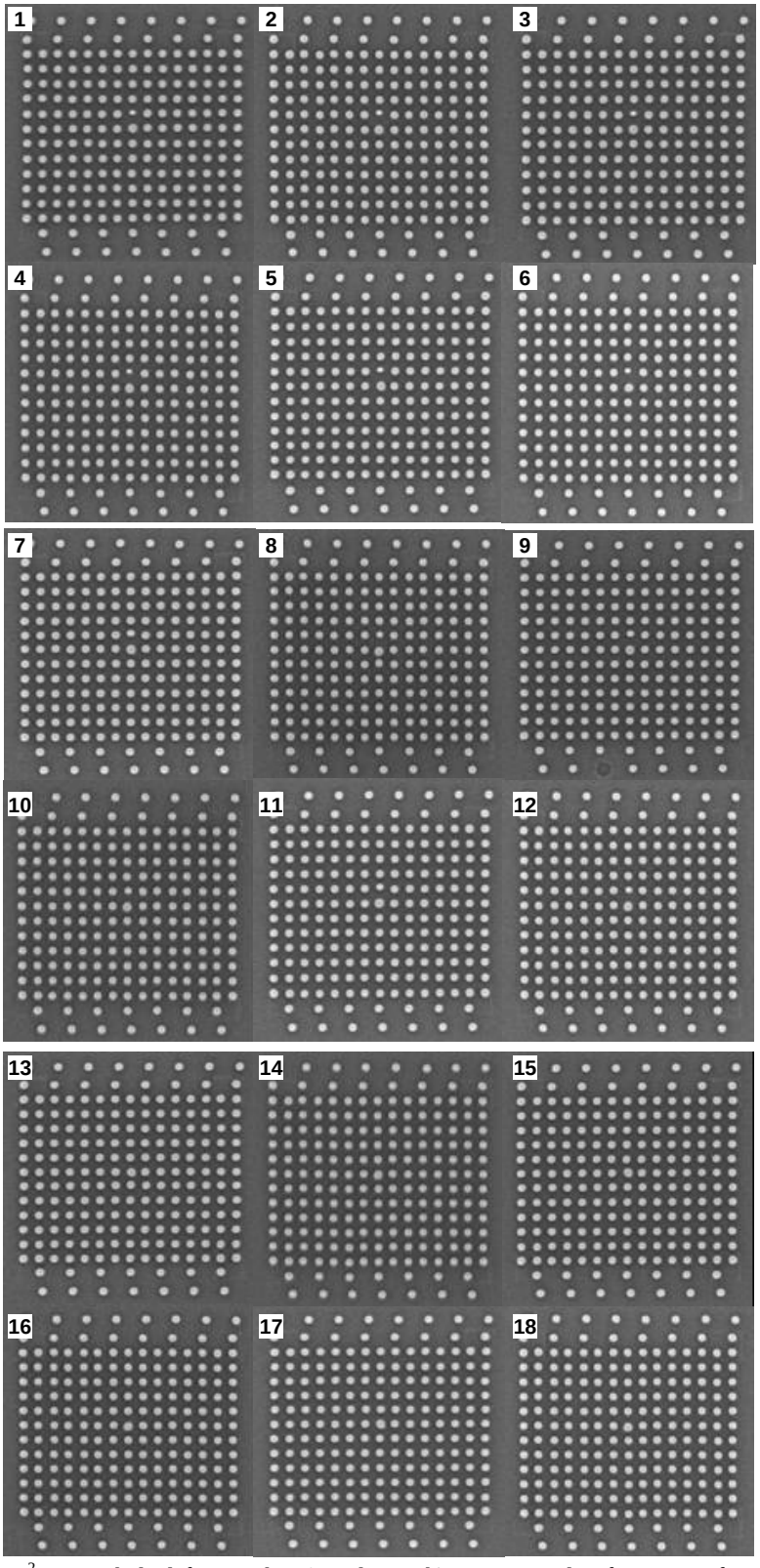

Figure 8. a) SEM image of repaired 40×40nm^2 contact hole defects in the 40nm design. b) Imprint results after repair of 18 different arrays with identical defect size.

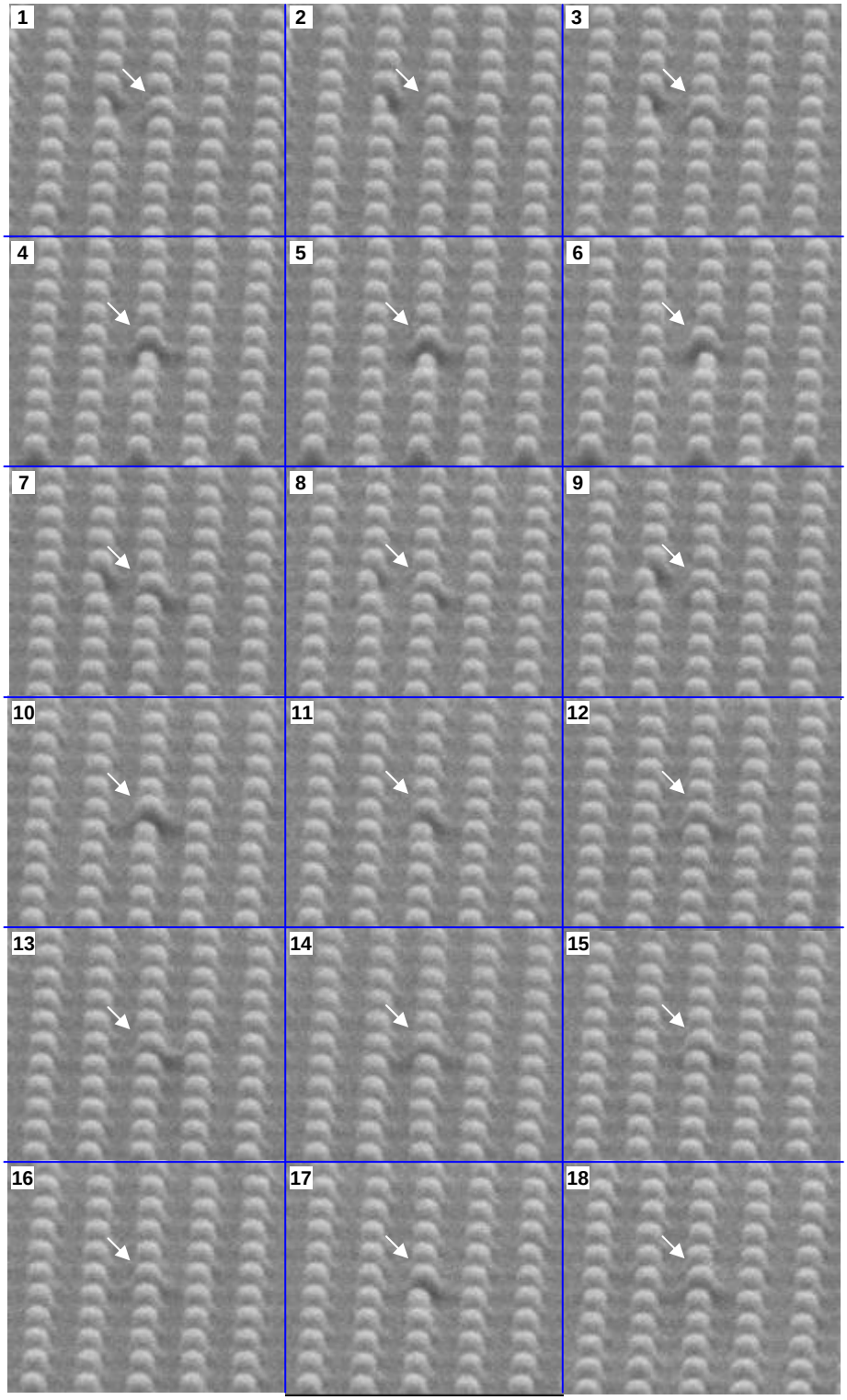

Figure 9. Imprinted pillar arrays after defect repair in the 40nm half pitch contact hole arrays on the template. All repaired pillars have equal shape and size and demonstrate the repeatability of the repair process.

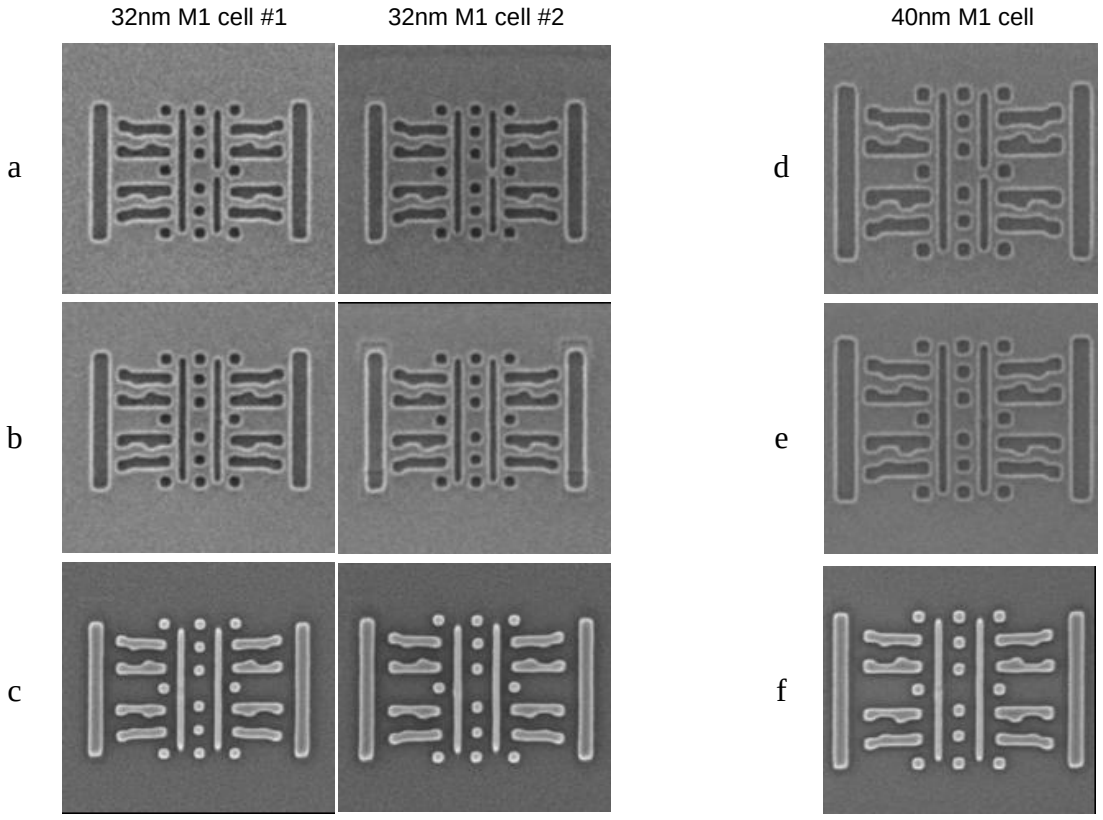

Figure 10. SEM images of two different 32nm SRAM Metal 1 cells with a $32\times32nm^2$ mousebite defect before repair (a), after repair (b) and the corresponding wafer imprint (c). The imprinted location of the defect is mirrored in x relative to the template image, because of the imprint process. Even for 32nm the repaired areas are well defined. These results demonstrate the capability of this technique for high-resolution defect repair. For comparison a 40nm Metal 1 pattern with a $40\times40nm^2$ mousebite defect is shown before repair (d), after repair (e) and the corresponding wafer imprint (f).